Structural and electrical characteristics of $Pb_{0.90}La_{0.15}TiO_3$ thin films on different bottom electrodes

S. Bhaskar, S. B. Majumder, P. S. Dobal, and R. S. Katiyar[a)]
Department of Physics, University of Puerto Rico, San Juan, PR-00931

S. B. Krupanidhi
Materials Research Center, Indian Institute of Science, Bangalore-560 030, India

$Pb_{0.90}La_{0.15}TiO_3$ (PLT15) thin films were deposited by the sol-gel method on Pt, Pt/Si, and RuO_2 on Si and Pt/Si bottom electrodes. X-ray diffraction, micro-Raman spectroscopy, and atomic force microscopy techniques were used for structural characterization of these films. PLT15 films on different electrodes showed good surface morphology with dense and uniform microstructure. PLT15 films on solution derived RuO_2 bottom electrodes show (100) preferred orientation of growth and result in larger crystallites. Films deposited on a Pt bottom electrode show sharp and intense Raman features indicating better crystallinity and insignificant film–electrode interactions. PLT15 film on a Pt bottom electrode exhibited higher dielectric constant (1300 at 100 kHz) and high values of P_m and P_r, 68 and 46 $\mu C/cm^2$, respectively, compared to other electrodes. Films on a RuO_2 bottom electrode showed relatively inferior dielectric and ferroelectric properties. The ac field dependence of dielectric permittivity at subswitching fields was fitted using the Rayleigh law. It was found that ~22% of the total measured permittivity was due to irreversible domain wall displacement for the films on a Pt electrode. The reversible polarization components estimated from the capacitance–voltage ($C-V$) and quasistatic hysteresis measurements showed that P_{rev}/P_{sat} at V_{max} for the case of Pt/Si (24%), was larger than that of Pt (11%) bottom electrodes. The observed results were correlated with the domain wall pinning at the disturbed film–electrode interface.

I. INTRODUCTION

Ferroelectrics are potentially important materials for various functional devices.[1,2] Lanthanum modified lead titanate (PLT) has been studied because of interest in their infrared sensing, electromechanical sensing, and actuating applications.[2–4] The incorporation of small amounts of La^{3+} into the perovskite structure, substituting by Pb^{2+} in lead titanate, reduces tetragonal distortion which, in turn, facilitates poling of the films and maintains a high value of the spontaneous polarization.[5] Because of their high dielectric constant and good ferroelectric properties, PLT thin films are an attractive material for applications in dynamic random access memories, ferroelectric random access memories, and various sensors.[2,6] Several growth methods, including rf-sputtering,[6] sol-gel,[7] pulsed laser deposition,[8] and chemical vapor deposition[9] were used to deposit PLT thin films. However the sol-gel route, a versatile method of preparing thin films, has several advantages, such as low processing temperature, nonvacuum process, low cost equipment required, and a uniform and large deposited surface area.

In determining the performance of a ferroelectric thin film capacitor, electrodes (especially the bottom electrode) play an important role because the structural and electrical properties such as leakage current, dielectric properties, surface roughness, fatigue, and thermal stability are strongly related to the nature and state of the bottom electrode.[10–13] Therefore several kinds of metal oxide and metallic compound electrodes have been suggested instead of the conventional pure metal electrodes. Numerous reports in the literature show that the RuO_2 bottom electrode reduced lattice mismatch and suppressed fatigue in ferroelectric thin films.[10–12,14,15] The solution deposition technique offers an alternative approach to synthesize high quality RuO_2 films.

We have prepared highly conductive, polycrystalline RuO_2 bottom electrodes on platinized silicon ($Pt/TiO_2/Si$) and silicon substrates. In the present study, we investigated the structural and electrical properties of PLT15 thin films on solution derived RuO_2 bottom electrodes on Pt/Si, Si substrates. These film properties are compared with those obtained using conventional Pt and Pt/Si bottom electrodes. The work attempts to address the nonlinear and hysteresis dielectric response of PLT15 thin films on a Pt electrode in terms of Rayleigh's law and show that the parameters are linearly frequency dependent on the applied ac field. Reversible and irreversible polarization contributions in the PLT15 thin films deposited on Pt and Pt/Si electrodes were compared and correlated with the film–electrode interface.

II. EXPERIMENTAL METHODS

A. Film preparation

The PLT15 precursor used in the present study was synthesized based on the chemical formula $Pb_{0.90}La_{0.15}TiO_3$ from lead acetate trihydrate, La-methoxyethanol, and Ti-isopropoxide. The details of the sol preparation are reported

[a)]Electronic mail: rkatiyar@rrpac.upr.clu.edu, Telephone: (787) 764 4210, Fax: (787) 7642571.

elsewhere.[16] The prepared sol was diluted with glacial acetic acid to a concentration of 0.25 M/L and used for coating. The sol was spun coated at 5000 rpm for 20 s to form a uniform gel film on various bottom electrodes. For the removal of organics, the deposited films were directly inserted into a furnace, preheated to a temperature of 650 °C. The coating and firing process was repeated to obtain films of about 1 μm thickness. Finally the films were annealed at 700 °C for crystallization into the perovskite phase. Both the firing and annealing operations were performed in flowing oxygen ambient.

The Pt bottom electrode used in our study was surface finished platinum foil (1.0 cm×0.5 cm×0.2 mm) obtained by hand polishing with alumina powder. Pt(400 nm)/TiO_2(100 nm)/SiO_2/Si substrates were commercially purchased from Radiant Tech. Inc. All substrates were cleaned with acetone and absolute alcohol prior to deposition of PLT15 thin films. $RuCl_3H_2O$ was used as a precursor material for preparing RuO_2 bottom electrodes on Si and Pt/Si substrates. Prior to film deposition, Si substrates were cleaned by ultrasonification in acetone and absolute alcohol. Pt/Si and Si substrates were spin coated with RuO_2 precursor solution, fired at 600 °C for 10 min and finally the films were annealed at 600 °C for 30 min in oxygen ambient; films so prepared were 0.7 μm thick. Details of the film preparation and characterization are described elsewhere.[17] Finally, PLT15 thin films were deposited on Pt, Pt/Si, RuO_2/Si, and RuO_2/Pt/Si substrates under similar experimental conditions.

B. Films characterization

Phase analysis was performed using a x-ray diffractometer (Siemens D5000) with Cu$K\alpha$ radiation (1.5405 Å). The crystallite sizes in the films were calculated from the x-ray diffractograms using Scherrer's equation.[18] The surface morphology of the films were imaged in noncontact mode using an atomic force microscope (AFM) (Nanoscope IIIa Multimode AFM Digital Instruments).

Raman measurements were performed using a Jobin-Yvon T64000 spectrophotometer consisting of a double premonochromator coupled to a third monochromator/spectrograph with 1800 grooves/mm grating. The 514.5 nm radiation of an Ar^+ laser was focused in a less than 2 μm diameter circle area by using a Raman microprobe with an 80× objective. The scattered light dispersed by the spectrophotometer was detected by a charge coupled device detection system. The Raman spectra were deconvoluted using the PEAKFIT program (Jandel Scientific Software).

For electrical measurements, Au top electrodes of 0.5 mm diameter were deposited on the surface of the PLT15 thin films. The dielectric properties of the films were then measured (1 kHz to 1 MHz) at room temperature with an impedance analyzer HP4294A (from Agilent Tech. Inc.). The polarization-electric field ($P-E$) hysteresis characteristics of PLT15 capacitors were obtained using the RT6000HVS ferroelectric tester (Radiant Tech. Inc.) in the virtual ground mode.

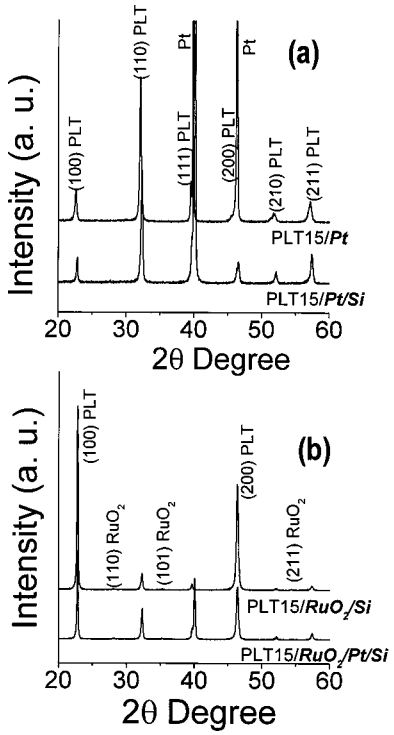

FIG. 1. The x-ray diffractograms of PLT15 thin film deposited on (a) Pt and Pt/Si and (b) RuO_2 on Si and Pt/Si bottom electrodes.

III. RESULTS AND DISCUSSIONS

A. Structural characterization

The structural and microstructural characteristics of PLT15 thin films on various bottom electrodes were studied using x-ray diffraction (XRD), micro-Raman, and AFM techniques. Figure 1 shows the x-ray diffractograms of PLT15 thin films deposited on (a) Pt and Pt/Si and (b) RuO_2 on Si and Pt/Si bottom electrodes. All the peaks in the x-ray are indexed with the film and substrate diffraction planes. XRD shows the single phase perovskite formation with no secondary phases of PLT15 thin film on various electrodes. Films deposited (annealed at 700 °C) on Pt and Pt/Si substrates exhibited a normal polycrystalline perovskite structure, with the main diffraction peaks characteristic of the (110) direction. The behavior was found to be consistent with that reported elsewhere[16] on PLT and other Pb based perovskite films. Figure 1(b) shows the XRD data obtained on PLT15 films deposited on RuO_2/Si and RuO_2/Pt/Si substrates. Both the films exhibited a preferred orientation along (100), even though the films were annealed at the same temperature of 700 °C, similar to the films on Pt and P/Si. This difference in the nature of crystallization can be attributed to possible differences in surface morphology, crystallite orientation, and the surface energy of Pt and RuO_2 bottom electrodes. It is also worth mentioning that no tetragonal split is evident in the XRD, which indicates the shifting of perovskite towards pseudocubic structure, possibly due to small grain size. Table I summarizes the crystallite size of the different films from the x-ray data using Scherrer's equation,[18] where β is the degree of preferred orientation expressed as $I_{(100)}/[\{I_{(100)}+I_{(110)}\}]$, and the lattice parameter values cal-

TABLE I. The crystallite size, β (the degree of preferred orientation $I_{(100)}/[\{I_{(100)}+I_{(110)}\}]$), and the lattice parameter values from the 2θ angle of x-ray diffraction planes for PLT15 thin films on various bottom electrodes.

Bottom electrodes	Crystallite size (Å)	β (%)	Lattice parameter (Å)
Pt	315	24	3.942
Pt/Si	291	20	3.915
RuO_2/Pt/Si	497	68	3.914
RuO_2/Si	464	85	3.914

culated assuming the psuedocubic nature of PLT15 thin films. Compared to the films on other electrodes, films deposited on Pt show slightly larger ''*a*'' values. This small variation in lattice parameter may be due to stress in the films from the bulk platinum substrate. In addition, films deposited on RuO_2 electrodes show larger crystallites and strong (100) preferred orientation.

Figure 2 shows the AFM image of PLT15 thin films on (a) Pt and (b) RuO_2/Si. Both images showed a similar surface morphology, with dense, uniform microstructure and low surface roughness (~2 nm). Films on a RuO_2/Si electrode show slightly larger grain growth compared with a Pt electrode. Overall films show good microstructure with no pinholes and microcracks. No significant change in the surface morphology was observed for the films deposited on other electrodes in the current regime of magnification.

Figure 3 shows the room temperature Raman spectra of the PLT15 thin films on various bottom electrodes in the 15–800 cm^{-1} region. The phonon modes observed in the spectrum are consistent with the C_{4v} space group of tetragonal phase in these films.[19] The films deposited on the Pt bottom electrode show sharp and intense Raman features, indicating better crystallinity and insignificant film–electrode interactions. However, the appearance of a Si peak at 521 cm^{-1} in the Raman spectra of the PLT15 film on the RuO_2/Si bottom electrode is indicative of Si diffusion into the film, leading to a poor film–electrode interface. Si diffusion into RuO_2 at higher processing temperatures has also been reported by other researchers[20] and affects the film–electrode interface, leading to relatively poorer dielectric and electrical properties.

The phonon peaks in the spectra were fitted to a damped harmonic oscillator model using the PEAKFIT program (Jandel Scientific Co.) and the following fitted parameters (a) peak frequencies, (b) integrated intensities, and (c) full width at half maximum (FWHM) of the $E(1TO)$, $A_1(1TO)$, $E(2TO)$, and $B+E$ phonons are plotted in Fig. 4 for various bottom electrodes. Both $A_1(1TO)$ and $E(1TO)$ phonons at $k=0$ in the tetragonal lead titanate originate from the vibrations of lead ion with respect to the slightly distorted TiO_6 octahedra.[21] The displacement polarization for $E(1TO)$ and $A_1(1TO)$ phonons lies along the ''*a*'' and ''*c*'' directions, respectively. The small decrease in the phonon frequencies $E(1TO)$ and $A1(1TO)$ modes for the Pt bottom electrode is due to the stress induced shift of the soft mode. This observation is supported by the x-ray lattice parameter calculation (Table II) from the shift in the 2θ angle of x-ray diffraction planes. The sharp (lower FWHM) and intense (larger integrated area) features of the Raman phonon modes indicate better crystallinity of the films and less film–electrode interface. A decrease in integrated intensity and in broad phonon features of the Raman bands provides a qualitative picture of the extent of the film–electrode interactions. Stronger interfacial reactions lead to more defects and change in the structure at the microscopic level and to reduced scattering intensity. Given the identical film preparation and stoichiometry, such changes in the Raman spectra could possibly be associated with the film–substrate interactions.

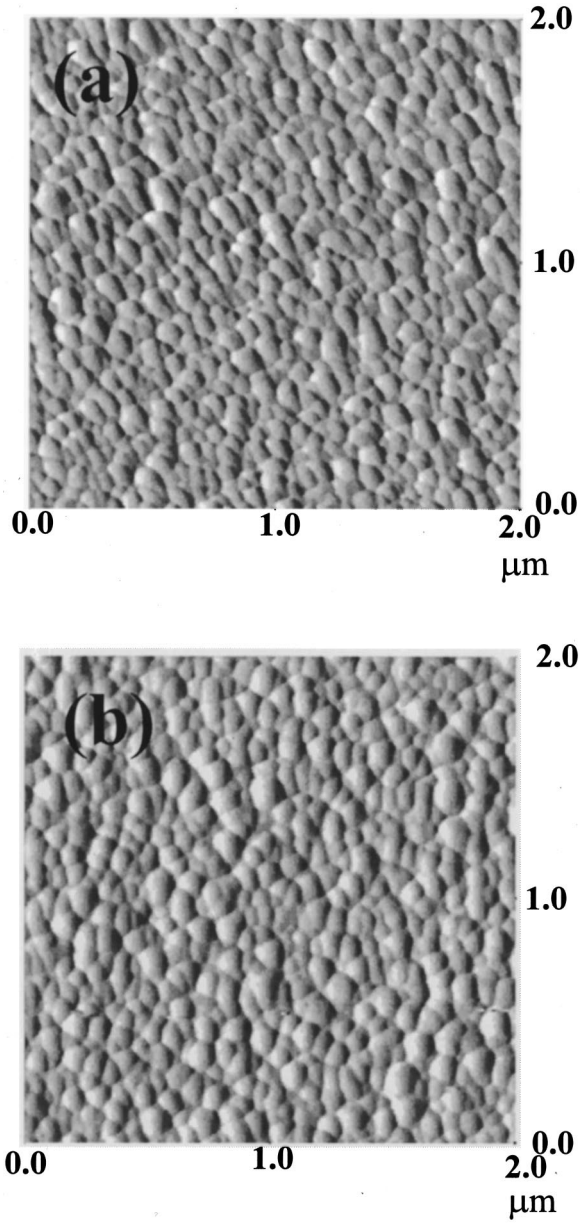

FIG. 2. The AFM images of PLT15 thin film deposited on (a) Pt and (b) RuO_2/Si electrodes.

B. Electrical characterization

1. Dielectric properties

Figures 5(a) and 5(b) show the dielectric constant and tangent loss as a function of frequency of PLT15 thin film on Pt, Pt/Si, and RuO_2 bottom electrodes. There is a drastic

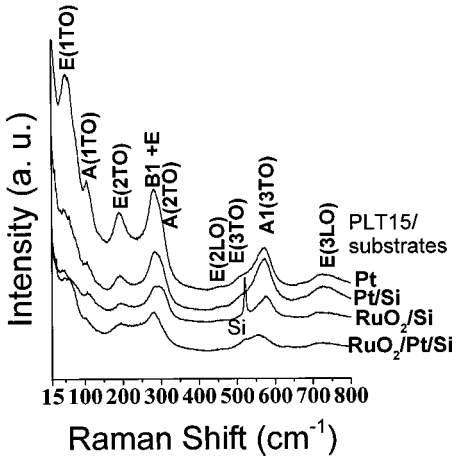

FIG. 3. The room temperature Raman spectra of the PLT15 thin films on various bottom electrodes in the 15–800 cm^{-1} region.

change in the dielectric properties of the films deposited on Pt and RuO_2 electrodes. Films deposited on Pt showed a high dielectric constant (1300 at 100 kHz) and low loss, while the films on the RuO_2 bottom electrode showed relatively inferior dielectric behavior. The reason for such a variation in dielectric property may be due to the presence of a disturbed layer at the film–electrode interface. This is possibly due to the thermal strain which occurs on annealing the samples, lattice mismatch, structural rearrangements in the course of crystallization, and chemical reactions at the interface, such as interaction with the silicon.[22] Results of Raman analysis also support that the presence of the disturbed layer is originating due to the chemical reactions at the RuO_2 electrode–film interface. The disturbed layer usually shows a lower dielectric constant, higher conductivity, and a high degree of disorder and it manifests itself in numerous traps and charge centers.[23,24] High dielectric constant and low loss in the PLT15 thin film on the Pt bottom electrode could be attributed to the insignificant presence of any interface layer in addition to better crystallization of the films, as supported by the sharp and intense features of Raman peaks.

Taylor and Damjanovic[25] reported the domain wall contribution to dielectric permittivity, under subswitching fields, in PZT thin films. We have investigated such phenomena in PLT15 films, measuring the frequency dependent dielectric behavior at different frequencies. PLT15 films on Pt substrate were chosen for this study because this combination showed a very insignificant influence by the interface. The dielectric data can therefore be analyzed more accurately. Figure 6 shows the ac field dependence of dielectric permittivity at 100 kHz frequency. Such behavior can be empirically described by a Rayleigh law as follows:

$$\varepsilon_{33}=\varepsilon_{\text{init}}+\alpha E_0, \tag{1}$$

where ε_{33} is the effective dielectric permittivity, E_0 is the magnitude of applied ac fields, and α is related to the irreversible polarization component.

The measured permittivities at different ac fields are shown as discrete points in Fig. 6. Using Eq. (1), a curve fit was performed to estimate the $\varepsilon_{\text{init}}$ and α parameters. The resulting parameters are $\varepsilon_{33}=1.608\times10^{-8}$ F/m and $\alpha=3.428\times10^{-15}$ F/V. In general, all the domains are expected to respond to the applied ac signal and contribute to the effective dielectric constant. However, due to the probable heterogeneity arising from the defects and the residual growth stresses, a few domains may not participate and are referred to as pinned domains.

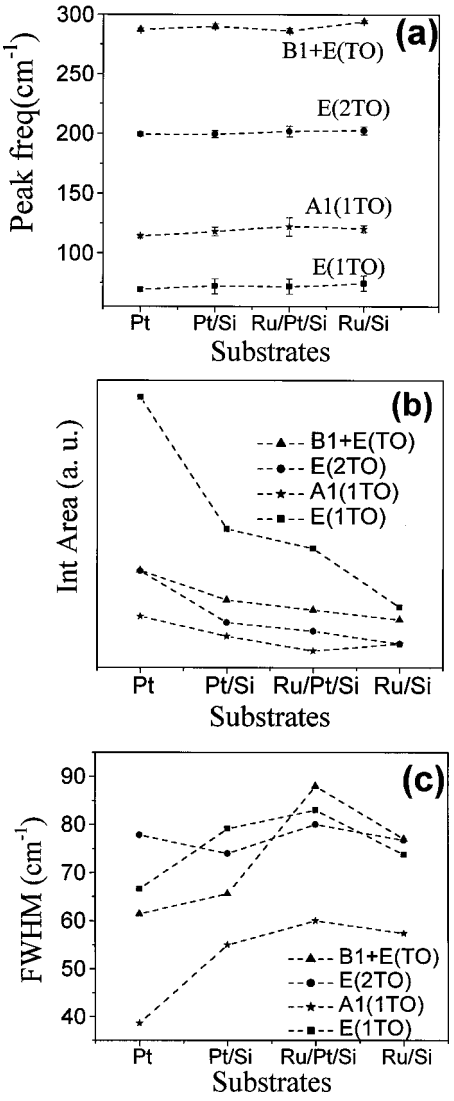

FIG. 4. The (a) peak frequencies, (b) integrated area, and (c) FWHM of the $E(1TO)$, $A_1(1TO)$, $E(2TO)$, and $B1+E$ phonons of Raman spectra of various bottom electrodes.

In terms of Rayleigh's law, $\varepsilon_{\text{init}}$ is due to an intrinsic lattice and the reversible domain walls displacement. The value of α obtained for PLT15 films (4.7×10^{-15} F/V) is

TABLE II. Maximum (P_m) and remnant ($\pm P_r$) polarization values of PLT15 thin films on various bottom electrodes from the $P-E$ hysteresis measurements.

Bottom electrodes	P_m (μC/cm^2)	P_r (μC/cm^2)	$-P_r$ (μC/cm^2)
Pt	68	46	−45
Pt/Si	55	24	−26
RuO_2/Pt/Si	32	10	−15
RuO_2/Si	12	4	−5

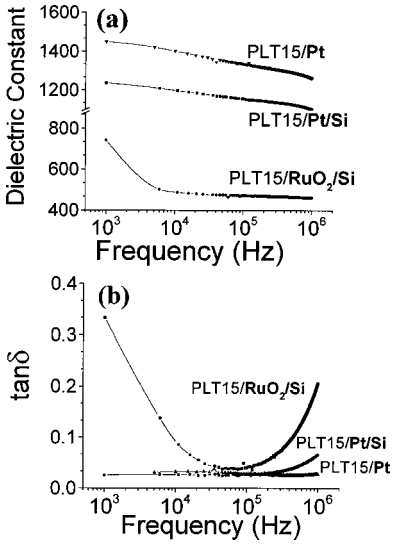

FIG. 5. (a) and (b) show the dielectric constant and tangent loss as a function of frequency of PLT15 thin film on Pt, Pt/Si, and RuO_2 bottom electrodes.

found to be higher by one order of magnitude than that reported for PZT films.[25] This may be due to the difference that in PLT films, the La substitution taken place in the *A*-site can bring in some intrinsic difference in domain wall behavior. Using the Rayleigh law, Eq. (1) the αE_0 (due to irreversible displacements of the domain walls), it was found that 22% of the total measured permittivity was due to irreversible domain wall displacement.

It has been shown that the pinning of the ferroelastic–ferroelectric domain walls on randomly distributed defects in ferroelectric ceramics leads to a field dependence of the piezoelectric coefficient that is analogous to the Rayleigh law for magnetic susceptibility.[26] Also that the piezoelectric coefficient of a lead zirconate titanate ferroelastic–ferroelectric system depends linearly on the logarithm of the frequency of the field. Such logarithmic frequency dependence of permittivity can be used to describe phenomenon related to pinning. Figure 7 shows the ac field dependent permittivity for a few frequencies ranging from 1 to 250 kHz selectively. The reversible ($\varepsilon_{\text{init}}$) and irreversible ($\alpha$) Rayleigh parameters at different frequencies could be obtained by fitting the data in

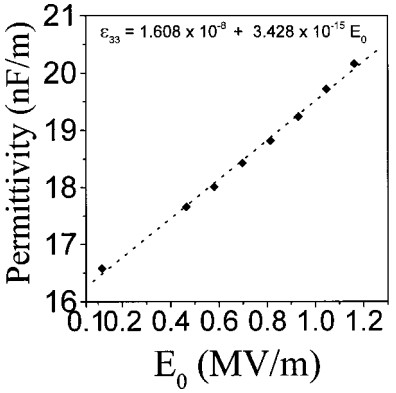

FIG. 6. Permittivity vs applied field at 100 kHz of PLT15 thin film on the Pt electrode.

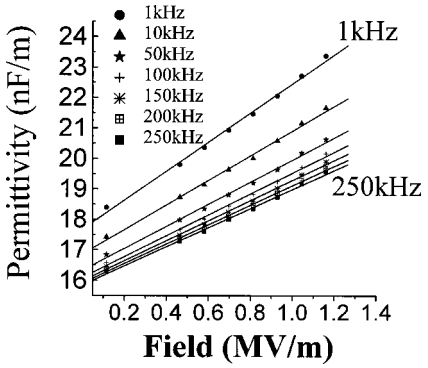

FIG. 7. Permittivity (ε_{33}) vs ac field E_0 for different frequencies. (Solid lines are fitted data and symbols indicate experimental data points.)

Fig. 7. The data obtained is plotted as a function of frequency in Fig. 8. The parameters were found to vary linearly with frequency, which may also be expressed as[24]

$$\varepsilon_{\text{init}} = e_0 - e \ln(\omega), \tag{2}$$

$$\alpha = a_0 - a \ln(\omega). \tag{3}$$

The resulting parameters are $e_0 = 1.76 \times 10^{-8}$ F/m, $e = 7.644 \times 10^{-10}$ F/m, $a_0 = 4.75 \times 10^{-15}$ F/V, and $a = 6.736 \times 10^{-16}$ F/m. The present results show that the logarithmic frequency dependence of the permittivity is due to the frequency dependence of both the reversible and irreversible Rayleigh parameters. This suggests that the irreversible component of the permittivity may be due to domain wall pinning.

2. Ferroelectric properties

Figure 9 shows the $P-E$ hysteresis loop of PLT15 thin films deposited on (a) Pt and (b) Pt/Si bottom electrodes. Films on Pt show good ferroelectric properties with high values of P_m and P_r, 68 and 46 μC/cm^2, respectively. Films on Pt/Si show lower polarization values and exhibit a nonsaturating behavior in the hysteresis loop. Table II summarizes the values of P_m and $\pm P_r$ for the PLT15 thin films deposited on Pt, Pt/Si, RuO_2/Pt/Si, and RuO_2/Si bottom electrodes. The $C-V$ measurements were performed at a frequency of 1 MHz with a different voltage ramp sweep for various bottom electrodes. Typical $C-V$ characteristics for the PLT15 thin films on various bottom electrodes are shown

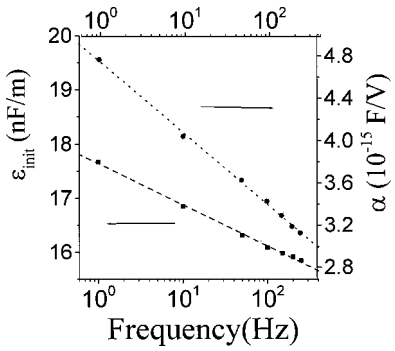

FIG. 8. Frequency dependence of the reversible ($\varepsilon_{\text{init}}$) and irreversible ($\alpha$) parameters. Solid lines indicate the best fits to Eqs. (2) and (3).

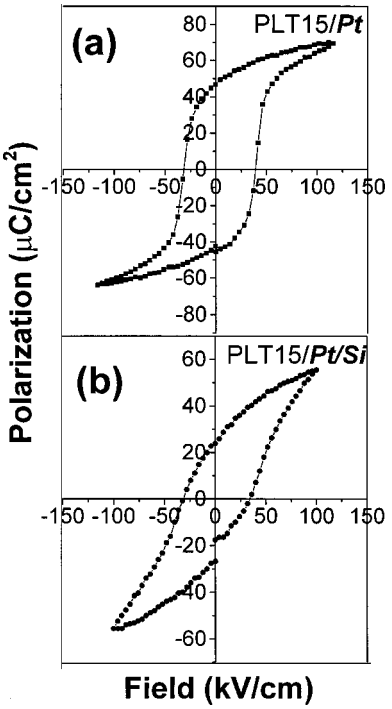

FIG. 9. $P-E$ hysteresis loops of PLT15 thin film on (a) Pt and (b) Pt/Si bottom electrodes.

in Fig. 10. The dependence of capacitance versus voltage has a strongly pronounced nonlinear character that is typical for ferroelectric materials.

To a first approximation the dependence of $C-V$ may be written as follows

$$C(V)=\varepsilon_{\text{lin}}\varepsilon_0 A/d+dP/dV, \tag{4}$$

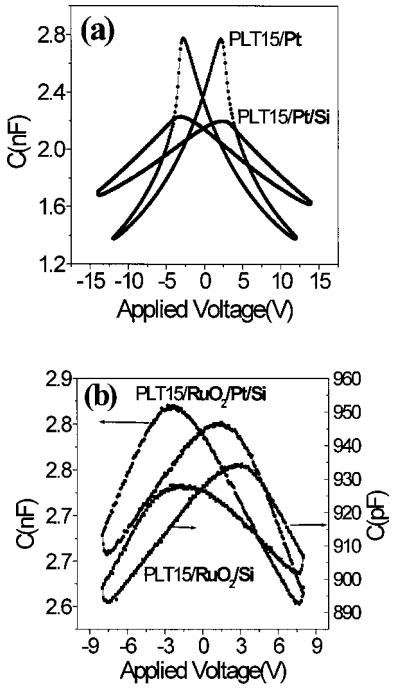

FIG. 10. Typical $C-V$ characteristics for the PLT15 thin film on various bottom electrodes.

where ε_{lin} is the linear dielectric constant, ε_0 is the dielectric constant, A is the electrode area, d is the film thickness, P is the polarization, and V is the voltage. The maximum values of capacitance are observed in the vicinity of the switching of the spontaneous polarization. With the increase in the applied field, the number of domains get decreased, the capacitance component in Eq. (4) for ferroelectric polarization decreases, and the capacitance of the structure is primarily determined by the linear capacitance component. The $C-V$ curves have lower asymmetry and relatively sharp features for the films on Pt and Pt/Si bottom electrodes due to the switching of the spontaneous polarization. A nonsaturating behavior was noticed for PLT15 films deposited on RuO_2 bottom electrodes. It was mentioned during the discussion of XRD and Raman results that a disturbed layer prevails at the film/substrate interface. Due to a lower dielectric constant of the interfacial layer, it is anticipated to have an accumulation of space charge.[24,27]

We have applied the technique adopted by Waser *et al.*[28] to separate the reversible and irreversible contributions to the total polarization. Small signal capacitance measurements under dc bias were used to measure the reversible contribution and quasistatic hysteresis mode measurements were used to obtain the total polarization (i.e., sum of reversible and irreversible contributions). The combination of both measurements allows the separation of the reversible and irreversible components of polarization.

Reversible contributions in ferroelectrics are due to the ionic and electronic displacements and to domain wall motions with a small amplitude. Irreversible processes can arise from either (a) lattice defects interacting with the domain wall or (b) the nucleation and growth of new domains or their combination. In addition, one cannot ignore the contributions of defect dipoles and free charges.[29] We have analyzed the samples of PLT15 films deposited on Pt and Pt/Si bottom electrodes to separate the reversible and irreversible polarization contribution. These samples were chosen for the study because they showed a very insignificant influence by the interface. Integrating the measured $C-V$ curves and dividing by the area of the electrodes using Eq. (5) one obtains the polarization curve, shown as an inset in Fig. 11.

$$P=1/A\int C(V)dV. \tag{5}$$

These curves reflect the reversible polarization contributions since the small ac signal (50 mV) superimposed on the slowly varying dc bias allows only for small, reversible displacements of the domain walls in the material. Figure 11 shows the measured quasistatic hysteresis curve that includes the sum of the reversible and irreversible contributions. By subtracting the reversible polarization (Fig. 11 inset) one obtains the irreversible polarization, as shown in Fig. 11(a) for Pt and (b) for Pt/Si electrodes.

From this analysis we could estimate the reversible polarization components in comparison with the total polarization at the maximum applied voltage. The $P_{\text{rev}}/P_{\text{sat}}$ at V_{max} for the Pt and Pt/Si substrates are 11% and 24%, respectively. The $P_{\text{rev}}/P_{\text{sat}}$ is larger for Pt/Si compared with the Pt bottom electrode. Thus these findings in conjunction with

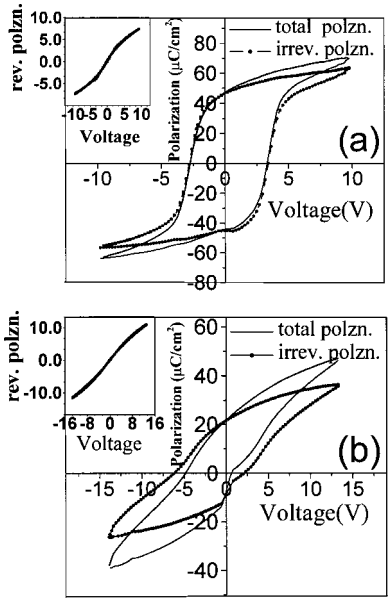

FIG. 11. Measured quasistatic hysteresis loops and the irreversible polarization obtained by subtracting the reversible contributions (shown in the inset) from $C-V$ curves for (a) Pt and (b) Pt/Si electrodes.

those from Raman and small signal ac measurements lead us to conclude that the presence of an effective interface layer has a significant impact on the polarization behavior in PLT15 films. More detailed analysis is underway to examine the effect of A-site substitution percentage on the reversible and irreversible components of domain walls and their role in polarizability.

IV. CONCLUSIONS

PLT15 thin films were deposited on Pt, Pt/Si, solution derived RuO_2/Si, and RuO_2/Pt/Si bottom electrodes. X-ray results established the single phase perovskite formation with no secondary phases of PLT15 thin film on different electrodes. Films deposited on RuO_2 bottom electrodes show (100) preferred growth orientation. AFM images showed surface morphology with dense uniform microstructure and low surface roughness for the films deposited on various electrodes. The sharp and intense features of Raman phonon modes of PLT15 thin films on Pt bottom electrodes indicated better crystallinity and less film–electrode interface. Films deposited on Pt showed high dielectric constant and low loss ($\varepsilon=1300$, $\tan\delta=0.028$ at 100 kHz), while the films on the RuO_2 bottom electrode showed relatively inferior dielectric behavior ($\varepsilon=470$, $\tan\delta=0.040$ at 100 kHz). Using the Rayleigh law, it was found that ~22% of the total measured permittivity was due to irreversible domain wall displacement for the films on the Pt electrode. The reversible ($\varepsilon_{\text{init}}$) and irreversible ($\alpha$) Rayleigh parameters were found to be frequency dependent. Films on the Pt bottom electrode showed good ferroelectric properties with high values of P_m and P_r, 68 and 46 μC/cm^2, respectively. Using $C-V$ and hysteresis loop analysis we estimated the reversible polarization components with respect to the total polarization for PLT15 thin films on Pt and Pt/Si, substrates were 11% and 24% respectively, at the maximum applied voltage ($P_{\text{rev}}/P_{\text{sat}}$ at $V_{\max}$). Thus these findings in conjunction with those from Raman and small signal ac measurements lead us to conclude that the presence of an effective interface layer has a significant impact on the polarization behavior in PLT15 films.

ACKNOWLEDGMENTS

The authors wish to thank Dr. Antonio Martinez for providing the x-ray facilities, A. L. M. Cruz for the AFM measurements, and Dr. Jo Taylor for critical reading of the manuscript. The work was partially supported by NSF-DMR No. 9801759, DAAG No. 55-98-1-0012, and NASA-NW88 grants.

[1] M. Okyama and Y. Hamakawa, Ferroelectrics **63**, 243 (1985).
[2] K. Ijima, R. Takayama, Y. Tomita, and I. Ueda, J. Appl. Phys. **60**, 2914 (1986).
[3] N. Nagao, T. Takeuchi, and K. Ijima, Jpn. J. Appl. Phys., Part 1 **32**, 4065 (1993).
[4] H. Adachi, T. Mitsuyu, O. Yamazaki, and K. Wasa, J. Appl. Phys. **60**, 736 (1986).
[5] T. Yamamota, H. Igarashi, and K. Okazaki, J. Am. Ceram. Soc. **66**, 363 (1983).
[6] R. Takayama, Y. Tomita, and I. Ueda, J. Appl. Phys. **63**, 5868 (1988).
[7] K. K. K. Soe, M. Maeda, and I. Suzuki, Jpn. J. Appl. Phys., Part 1 **35**, 205 (1996).
[8] S. B. Xiong, Z. G. Liu, and N. Xu, Ferroelectrics **195**, 171 (1997).
[9] J. C. Shin, J. M. Lee, S. K. Hong, H. J. Cho, K. S. Kim, C. S. Hwang, and H. J. Kim, J. Vac. Sci. Technol. A **16**, 2591 (1998).
[10] D. P. Vijay and S. B. Desu, J. Electrochem. Soc. **140**, 2640 (1993).
[11] H. Maiwa, N. Ichinose, and K. Okazaki, J. Appl. Phys. **33**, 5223 (1994).
[12] H. N. Lee, Y. T. Kim, and S. H. Choh, Ferroelectrics **197**, 97 (1997).
[13] M. S. Tsai, S. C. Sun, and T. Y. Tseng, IEEE Trans. Electron Devices **46**, 1829 (1999).
[14] K. Sreenivas, I. Reaney, T. Maeder, N. Setter, C. Jagadish, and R. G. Elliman, J. Appl. Phys. **75**, 232 (1994).
[15] W. I. Lee, J. K. Lee, J. S. Lee, and I. K. Yoo, Integr. Ferroelectrics **10**, 145 (1995).
[16] S. B. Majumder, S. Bhaskar, P. S. Dobal and R. S. Katiyar, Integr. Ferroelectrics **23**, 127 (1999).
[17] S. Bhaskar, S. B. Majumder, P. S. Dobal, A. L. M. Cruz, E. R. Fachini, and R. S. Katiyar, Mater. Res. Soc. Symp. Proc. **606**, 211 (1999).
[18] D. Cullity, *Elements of X-ray diffraction* (Addition-Wesley, Reading, MA, 1967), p. 261.
[19] G. Burns and B. A. Scott, Phys. Rev. Lett. **25**, 1191 (1970).
[20] J. F. Tressler, K. Watanabe, and M. Tanaka, J. Am. Ceram. Soc. **79**, 525 (1996).
[21] J. D. Freire and R. S. Katiyar, Phys. Rev. B **37**, 2074 (1988).
[22] S. P. Muraka, *Silicides for VLSI Applications* (Academic, Orlando, 1983), p. 103.
[23] J. C. Burfoot and G. W. Taylor, *Polar Dielectrics and Their Applications* (Macmillan, London, 1979).
[24] K. A. Vorotilov, M. I. Yanovskaya, and O. A. Dorokhova, Integr. Ferroelectrics **3**, 33 (1993).
[25] D. V. Taylor and D. Damjanovic, J. Appl. Phys. **82**, 1973 (1997).
[26] D. Damjanovic, Phys. Rev. B **55**, 649 (1997); J. Phys. D **29**, 2057 (1996).
[27] S. Y. Wu, IEEE Trans. Electron Devices **ED-21**, 499 (1974).
[28] D. Bolten, U. Bottger, M. Grossmann, O. Lohse, R. Waser, M. Kastner, G. Schindler and C. Dehm, Mater. Res. Soc. Symp. Proc. **596**, 301 (2000).
[29] D. Bolten, O. Lohse, M. Grossmann, and R. Waser, Ferroelectrics **221**, 251 (1999).